Check for updates

ADVANCED ELECTRONIC MATERIALS
www.advelectronicmat.de

Charge Traps in All-Inorganic $CsPbBr_3$ Perovskite Nanowire Field-Effect Phototransistors

*Felix Winterer, Lisa Sophie Walter, Jakob Lenz, Stefan Seebauer, Yu Tong, Lakshminarayana Polavarapu, and Ralf Thomas Weitz**

All-inorganic halide perovskite materials have recently emerged as outstanding materials for optoelectronic applications. However, although critical for developing novel technologies, the influence of charge traps on charge transport in all-inorganic systems still remains elusive. Here, the charge transport properties in cesium lead bromide, nanowire films are probed using a field-effect transistor geometry. Field-effect mobilities of $\mu_{FET} = 4 \times 10^{-3}$ cm^{-2} V^{-1} s^{-1} and photoresponsivities in the range of $R = 25$ A W^{-1} are demonstrated. Furthermore, charge transport both with and without illumination is investigated down to cryogenic temperatures. Without illumination, deep traps dominate transport and the mobility freezes out at low temperatures. Despite the presence of deep traps, when illuminating the sample, the field-effect mobility increases by several orders of magnitude and even phonon-limited transport characteristics are visible. This can be seen as an extension to the notion of "defect tolerance" of perovskite materials that has solely been associated with shallow traps. These findings provide further insight in understanding charge transport in perovskite materials and underlines that managing deep traps can open up a route to optimizing optoelectronic devices such as solar cells or phototransistors operable also at low light intensities.

1. Introduction

Halide perovskite materials have emerged as a promising new class of semiconductor materials for optoelectronic applications owing to their attractive optical and electronic properties such as high absorption coefficients[1,2] and long charge carrier lifetime,[3] together with ease of fabrication, solution processability and low cost.[4] They have shown great promise and potential in various applications such as solar cells,[3,5] photodetectors,[6–8] field-effect transistors (FETs),[9–12] and lasers.[13] However, the performance of halide perovskite devices is often limited by insufficient stability and moderate crystallinity. In the last years, significant advance has been achieved by the extension of perovskite materials into (all-inorganic) colloidal nanocrystals.[4] Here, the shape and composition of perovskite nanocrystals are easily controllable and a wide range of morphologies have been synthesized.[4,14–17] Among all, especially perovskite nanowires (NWs) show great promise for high performance optoelectronic devices such as lasers and photodetectors.[8,13,18] However, to exploit the full potential of halide perovskite materials, profound understanding of the microscopic transport mechanisms is prerequisite. For example, a better understanding of the influence of charge traps and the often cited "defect tolerance"[19–23] of perovskite materials can provide crucial information for optimizing charge generation and transfer in perovskite solar cells.[21] Here, FETs are a versatile platform to investigate charge transport in semiconductor

F. Winterer, L. S. Walter, J. Lenz, S. Seebauer, Prof. R. T. Weitz
Physics of Nanosystems, Department of Physics
Ludwig-Maximilians-University Munich
Geschwister-Scholl-Platz 1, 80799 Munich, Germany
E-mail: thomas.weitz@uni-goettingen.de

Dr. Y. Tong, Dr. L. Polavarapu
Chair for Photonics and Optoelectronics
Nano-Institute Munich
Department of Physics
Ludwig-Maximilians-University Munich
Königinstrasse 10, 80539 Munich, Germany

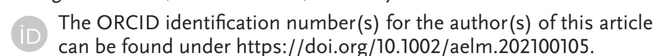
The ORCID identification number(s) for the author(s) of this article can be found under https://doi.org/10.1002/aelm.202100105.

© 2021 The Authors. Advanced Electronic Materials published by Wiley-VCH GmbH. This is an open access article under the terms of the Creative Commons Attribution-NonCommercial License, which permits use, distribution and reproduction in any medium, provided the original work is properly cited and is not used for commercial purposes.

DOI: 10.1002/aelm.202100105

Dr. L. Polavarapu
CINBIO, Materials Chemistry and Physics Group
Department of Physical Chemistry
Universidade de Vigo
Campus Universitario Lagoas
Marcosende, Vigo 36310, Spain

Prof. R. T. Weitz
Center for Nanoscience (CeNS)
Schellingstrasse 4, 80799 Munich, Germany

Prof. R. T. Weitz
I. Physical Institute
Faculty of Physics, Georg-August-University Göttingen
Friedrich-Hund-Platz 1, 37077 Göttingen, Germany

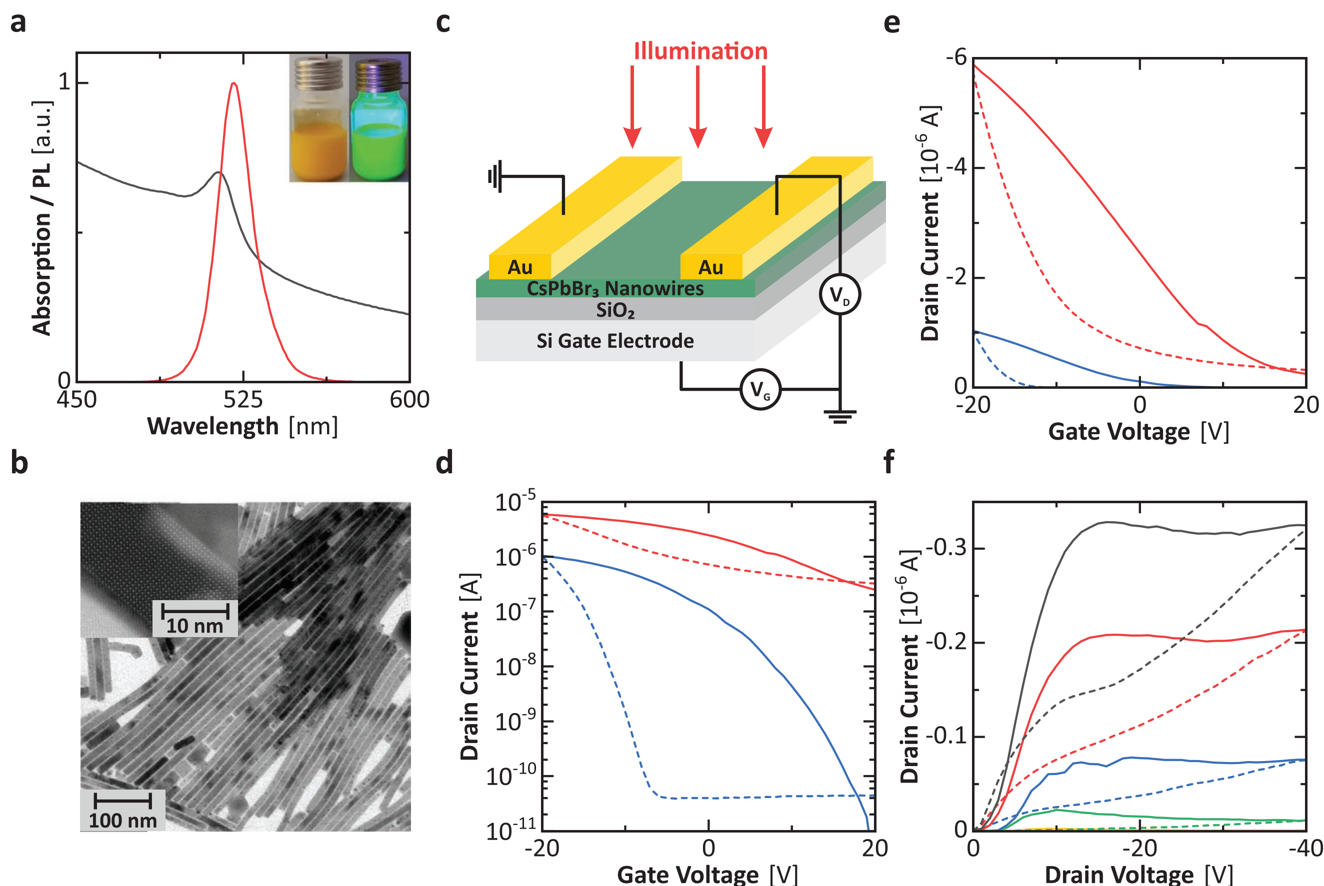

Figure 1. Spectroscopy and field-effect transistor characteristics: a) UV–visible extinction (black) and photoluminescence (red) spectra of the colloidal $CsPbBr_3$ NWs. The inset shows images of the colloidal solutions of $CsPbBr_3$ NWs under white light (left) and UV illumination (right). b) Bright-field transmission electron microscopy image and high-angle annular dark-field scanning transmission electron microscopy image (inset) of the $CsPbBr_3$ NWs. c) Schematic of the device architecture. The p-doped Si substrate acts as a back-gate, while the two gold pads serve as drain and source electrodes. The perovskite and the gate electrode are separated by a SiO_2 dielectric. d,e) Transfer curves at $V_D = -20$ V with illumination (red) and without (blue) in logarithmic (d) and linear (e) scaling. The solid lines show the forward sweep and the dotted lines the backward sweep. f) Output curves without illumination. Gate voltages range from $V_G = 0$ V (yellow) to $V_G = -40$ V (black) in increments of 10 V. The solid lines represent the forward sweeps and the dotted lines the backward sweeps.

materials. Unlike in solar cells, the FET geometry allows to explore the influence of traps on charge carrier mobility both with and without illumination. Starting from the pioneering work on layered hybrid tin halide perovskites[24] to experiments on methylammonium lead halide perovskites (MALHs)[9–11,25,26] to all-inorganic perovskite FETs,[12,27–29] several studies aiming to unveil transport mechanisms in perovskite materials have been conducted. Yet, especially for inorganic or nanocrystal-based materials, thorough studies of transport mechanisms and the influence of traps are still lacking.

In this work, we fabricated $CsPbBr_3$ nanowire phototransistors and investigated their temperature-dependent transport properties both in the dark and under illumination down to cryogenic temperatures. We demonstrate maximum field-effect mobilities of $\mu_{FET} = 4 \times 10^{-3}$ cm^{-2} V^{-1} s^{-1} and room temperature responsivities of $R = 25$ A W^{-1} at a power density of 3.9 mW cm^{-2}. Furthermore, temperature-dependent measurements enabled us to determine both depth and density of deep and shallow traps in the presented system. Surprisingly, investigating the gate-dependent photoconductivity revealed metal-like transport characteristics even in the presence of an appreciable density of deep traps. This intriguing observation again underlines the notion of "defect tolerance" in perovskite systems and even extends it to deep traps.

2. Results

The colloidal $CsPbBr_3$ NWs were prepared by a ligand-assisted ultrasonication approach (see Experimental Section for the synthesis details). The UV–visible absorption and photoluminescence spectra of $CsPbBr_3$ NWs are depicted in **Figure 1**a. The prepared $CsPbBr_3$ NWs exhibit an excitonic absorption peak at 513 nm and photoluminescence peak at 525 nm. The colloidal solution of NWs emits intense green emission under UV illumination (inset of Figure 1a). TEM analysis of the NWs shows that they have a diameter of 12 nm and length ranging from 0.5 to 2 µm (Figure 1b). The NWs are single crystalline as revealed by HAAD-STEM analysis (inset of Figure 1b). To analyze electrical transport properties of the $CsPbBr_3$ nanowire thin films,

 © 2021 The Authors. Advanced Electronic Materials published by Wiley-VCH GmbH

the perovskite nanowire solution was spin-coated onto a Si/SiO_2 substrate and bottom-gate top-contact FET devices were fabricated (see Experimental Section for fabrication details). Figure 1c shows the schematic illustration of the device architecture. In the following, the data of three devices on one exemplary sample (sample A) is presented. Data of further devices and samples is shown in the Supporting Information (see Table S1, Supporting Information, for a sample overview). The layer thickness of the nanowire film was measured to be 530 nm thick with an RMS roughness of ≈60 nm (see Figure S1, Supporting Information, for more details on the topology of the sample). Thus, the electrical measurements can be seen as an ensemble average over many NWs. All electrical measurements were taken in vacuum below 5×10^{-7} mbar. Measurements in bright illumination conditions were done by illuminating the sample with a broadband halogen lamp with a power density of 3.9 mW cm^{-2}. First, transfer curves for several FET devices with a constant drain voltage of $V_D = -20$ V and gate voltages V_G ranging from −20 to +20 V in both dark and bright illumination conditions were recorded. Figure 1d,e shows the transfer curves of one exemplary device both with and without illumination. Other devices qualitatively show the same behavior (see Figure S2, Supporting Information). Additionally, Figure 1f shows the output curves of the device for drain voltages up to $V_D = -40$ V. Without illumination, transfer and output curves show a clearly visible field-effect with a current modulation over several orders of magnitude.

The devices show a distinct p-type semiconducting behavior, where only hole conduction is present and can be modulated with the gate voltage. Electron transport, on the other hand, is completely suppressed throughout the entire accessible gate range. The absence of electron transport has already been seen in other $CsPbBr_3$ samples,[27–29] whereas in some $CsPbBr_3$ devices ambipolar transport was observed.[12] These inconsistent observations can be explained by varying trap concentrations in the respective samples caused by different growth conditions.[19,30,31] A high density of traps close to the valence band, for example, can lead to a shift of the electron conductivity onset to high positive voltages exceeding the accessible gate range. Such traps can be associated with vacancies of Cs and Pb that have particularly low formation energies in Br-rich growth conditions.[19,21] In addition to the p-type conductivity, both output and transfer curves display a pronounced "clockwise" hysteresis between forward and reverse sweeps. This strong hysteresis is very common for perovskite materials and has been broadly reported for perovskite FETs and solar cells, even for single crystal samples.[9–12,25–28,32] Possible explanations for the hysteresis include ion migration, ferroelectricity, trap states in the material, and surface traps at the interface to the dielectric.[10–12,25–28] Although there is still much debate on the microscopic cause of hysteresis, screening of the gate potential due to mobile ions has been widely regarded as the dominant mechanism at room temperature.[11,12,25,28,33] However, also traps at the dielectric interface can give rise to substantial hysteresis.[34] Ferroelectricity, on the other hand, showed only minor influence on electrical transport.[11,33,35] At low temperatures, ion migration is expected to be suppressed due to high activation energies[11,12,25,28,33,36–38] and interface traps are widely believed to become the dominant mechanism leading to hysteresis.[11,12,25,33] As temperature-dependent measurement can help to shed more light onto the causes of hysteresis, we will revisit this discussion later. Based on the output and transfer curves, we have estimated the FET mobility in the saturation regime to be $\mu_{FET}^{Dark} = 4 \times 10^{-3}$ cm^2 V^{-1} s^{-1} at room temperature for our best device (see Supporting Information and Figure S3, Supporting Information, for more details). In this calculation, only the forward sweep was used as the reverse sweep tends to yield unreliable results due to the strong hysteresis effect.[11] In other $CsPbBr_3$ systems higher FET mobilities with record values of up to 2.2 cm^2 V^{-1} s^{-1} at room temperature have been reported.[12,28,29,39] However, even these record mobilities are still at well below what has been expected from time-resolved photoluminescence measurements,[7,40] acousto–optoelectronic spectroscopy,[41] Hall-effect measurements,[36,42] and THz spectroscopy.[43] Thus, a better understanding of the underlying transport mechanisms bears great potential for optimizing mobilities of all-inorganic perovskite devices.

A distinctly different behavior can be observed when illuminating the sample with a halogen lamp. As shown in Figure 1d, when switching on the illumination, the drain current increases significantly by up to four orders of magnitude. Since there is still a field effect present, the charge carrier mobility can be obtained similar to dark case. For our best device, the mobility of the illuminated devices is $\mu_{FET}^{Bright} = 1.8 \times 10^{-2}$ cm^2 V^{-1} s^{-1}. The increase of mobility during illumination is consistent with observations on other perovskite devices.[12,28] In general, the strong photoconductivity is directly connected to the combination of excellent optical absorption characteristics and efficient charge transport properties of perovskite materials.[2,3,20] Due to the high absorption coefficient, photo-excited charge carriers are generated very efficiently.[3] At the same time, fast exciton dissociation[1,2,44] as a result of the low exciton binding energies[1,20,44] leads to a high population of free charge carriers.[1,2,45] These free carriers can then contribute to the transport through the material and enhance the conductivity irrespective of the gate voltage.[6,12,46] This phenomenon is known as the photoconductive effect and leads to a vertical shift of the transfer curves to higher drain currents.[6,12,46] The quasi-additive behavior of a constant photocurrent onto a gate-tunable current[46] agrees well with our measurement data. Notably, the emergence of the photoconductive effect also implies that both mobile holes and mobile electrons are present in the system. This is very surprising, as electrons were completely immobilized in local trap states in the dark and only holes were mobile. Furthermore, the photocurrent is suppressed by more than one order of magnitude when illuminating the sample with light at excitation energies below the band gap (1.91 eV) compared to above the band gap (2.33 eV). Thus, charge carriers are indeed photo-excited within the material rather than at the contacts or nanowire interfaces. The transfer curves also allow for calculating the photoresponsivity, R (drain current increase per illumination power), of the devices.[6,46] For our best device, we achieve photoresponsivities of $R = 25$ A W^{-1} upon broadband white light illumination with a power density of 3.9 mW cm^{-2}. This compares very well even to single crystal $CsPbBr_3$ samples with responsivities of up to several hundred A W^{-1} at comparable power densities.[7,8,12,47] The maximum specific detectivity in the shot-noise limit[12] reaches values of $\approx 1 \times 10^{13}$ Jones at this power density. The gate dependence of both resistivity and detectivity is shown in Figure S4, Supporting Information.

 © 2021 The Authors. Advanced Electronic Materials published by Wiley-VCH GmbH

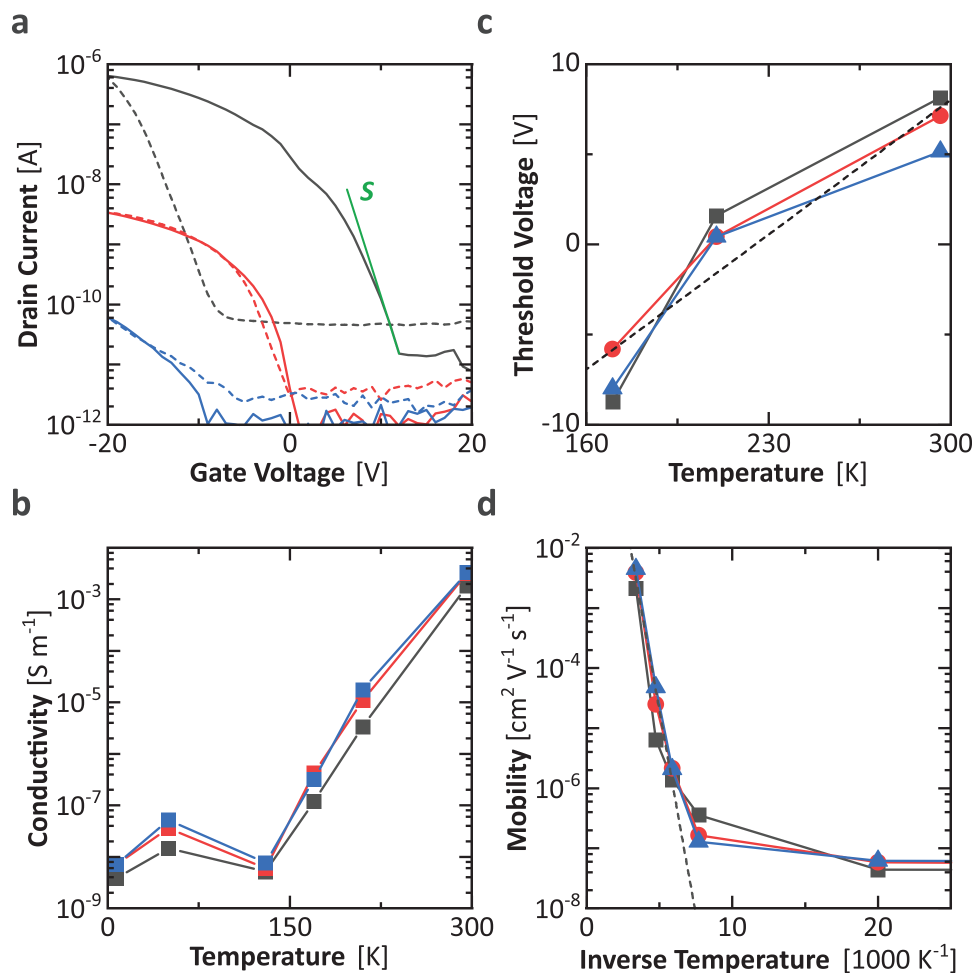

Figure 2. Temperature-dependent transport without illumination: a) Transfer curves at $T = 296$ K (black), $T = 210$ K (red), and $T = 170$ K (blue) at a drain voltage of $V_D = -20$ V. The solid lines show the forward sweep and the dotted lines the backward sweep. The determination of the subthreshold swing, S, is indicated by the green line. b) Maximum conductivity of three different devices (black, red, and blue) as a function of temperature. The conductivity fluctuations close to zero are due to limitations of the measurement. c) Threshold voltage of three different devices (black, red, and blue) as a function of temperature. The linear fit to the data points is represented by the black dotted line. d) Arrhenius plot of the mobility of three different devices (black, red, and blue) with respect to the inverse temperature. A fit to the first few data points is shown as a black dotted line. The lower limit of the mobility at higher temperatures is due to limitations of our measurement system.

In order to investigate the influence of traps in more detail, the electrical transport properties of the $CsPbBr_3$ NWs were measured as a function of temperature. At discrete temperature steps between 296 and 8 K, transfer curves for both dark and bright illumination conditions were obtained. **Figures 2** and **3** show the transport characteristics at various temperatures without and with illumination, respectively. First, it can readily be seen, that without illumination both conductivity and mobility decrease substantially with decreasing temperature. This mobility freeze-out indicates a thermally activated behavior originating from charge traps in the material[48–51] or Schottky barriers at the electrode–perovskite interface.[50–52] In general, Schottky barriers emerge due to the energy mismatch of valence and conduction band to the work function of the electrodes. However, the weak dependence of the conductivity on temperature in illuminated samples indicates that charge transport is dominated by charge traps rather than barrier physics. At this point, it is also worth discussing further mechanisms that could potentially influence temperature-dependent transport properties, namely ion migration and perovskite phase transitions. First, as mentioned earlier, mobile ions can effectively screen the gate potential and, thus, lead to hysteresis.[11,12,25,28,33] When decreasing the temperature, ion migration is expected to freeze out and the hysteresis is suppressed.[11,28] In our devices, almost no hysteresis is visible in the transfer curves at 210 K (see Figure 2a). Thus, we believe ion migration cannot explain the observed mobility suppression and can be neglected for temperatures $T \leq 210$ K.[11,28,36] The same is true for interfacial traps at the dielectric, that would lead to a similar hysteretic behavior.[34] Second, MALH systems are subject to a structural phase transition from orthorhombic to tetragonal crystal structure at around $T_C = 160$ K that can significantly alter electronic properties of the system.[10,25] However, the phase transition temperature of $CsPbBr_3$ is well above room temperature, namely at $T = 361$ K from orthorhombic to tetragonal and at $T = 404$ K to cubic crystal structure.[53,54]

© 2021 The Authors. Advanced Electronic Materials published by Wiley-VCH GmbH

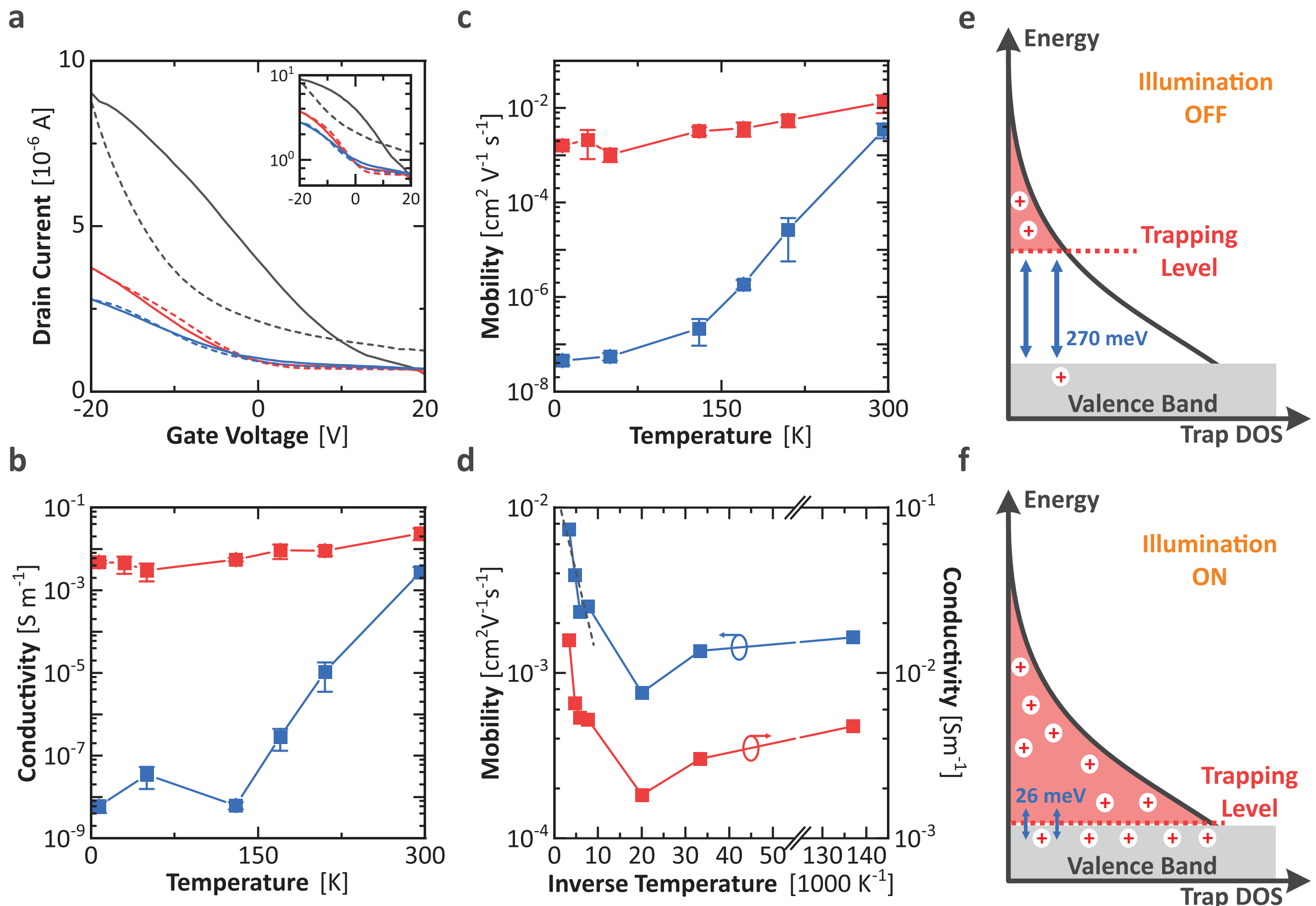

Figure 3. Temperature-dependent transport under illumination: a) Transfer curve in linear and logarithmic (inset) scaling for temperatures $T = 296$ K (black), $T = 210$ K (red), and $T = 8$ K (blue). The solid lines represent the forward sweep and the dotted lines the backward sweep. b) Comparison of the conductivity with illumination (red) and without (blue) with respect to the temperature averaged over three different devices. The gate voltage was set to $V_G = -20$ V. The conductivity fluctuations close to zero are due to limitations of the measurement. c) Comparison of the mobility with illumination (red) and without (blue) with respect to the temperature averaged over three different devices. d) Comparison of mobility and conductivity with illumination with respect to the inverse temperature. The fit of the Arrhenius relation to the mobility is shown as a black dotted line. e,f) Schematic trap density of states with the trap filling level (red) for dark (e) and illuminated (f) samples. In the dark, only deep traps are filled and transport is dominated by thermally activated behavior with a high activation energy. In illuminated samples, almost all traps are filled and only shallow traps influence charge transport.

Therefore, a phase transition is not present in the investigated temperature range.

In the following, properties of the charge traps are investigated in more detail and light is shed onto the often cited "defect tolerance" of perovskites.[19,21] In this context it is very instructive to distinguish between shallow traps close to the band edge ($\Delta E \approx k_B T$) and deep traps far away from the band edge ($\Delta E \gg k_B T$).[21,49] First, we estimated the trap density of deep traps based on the subthreshold swing, S, of the transfer curves using the formulas[12,49,55]

$$S = \frac{dV_{GS}}{d(\log I_{SD})}$$

$$N_{DT} = \left(\frac{C}{e}\right)\left(\frac{eS}{k_B T \ln 10} - 1\right) \tag{1}$$

where e is the elementary charge, k_B the Boltzmann constant, T the temperature, and C the gate dielectric capacitance per unit area. An illustration of the subthreshold swing determination is shown in Figure 2a. This yields an average deep trap density of $N_{DT} = 7 \times 10^{12}$ cm^{-2} eV^{-1} at room temperature. This trap density is smaller than trap densities reported in literature even for single crystal samples.[12,22] As the Fermi level is still far away from the band edge in the subthreshold regime, the density N_{DT} can be associated with deep trap states.[49] The density N_{ST} of shallow trap states closer to the band edge can be estimated from the dependence of the threshold voltage on the temperature using[49,55]

$$N_{ST} = \left(\frac{C}{ek_B}\right)\frac{dV_{th}}{dT} \tag{2}$$

This gives a trap density of $N_{ST} = 3 \times 10^{14}$ cm^{-2} eV^{-1} in our system. Figure 2c shows the calculated threshold voltages with respect to the temperature together with the line fit used to determine N_{ST}. With the gate voltage, a maximum

© 2021 The Authors. Advanced Electronic Materials published by Wiley-VCH GmbH

ADVANCED ELECTRONIC MATERIALS
www.advelectronicmat.de

charge carrier density of $n_{Gate} = 4 \times 10^{12}$ cm^{-2} can be induced. Thus, the gate is very likely not sufficient to fill even the deep traps in the system and transport is expected to be trap dominated. This is consistent with the distinct thermally activated behavior of the mobility as shown in Figure 2d. Fitting an Arrhenius relation, $\mu \approx \exp(-E_A/k_BT)$, to the temperature dependence of the mobility yields an approximate measure of the trap depth.[48,49,51,55] In the dark and for temperatures above $T \geq 170$ K, the fit reveals a surprisingly deep trap depth (activation energy) of $E_A = 270 \pm 16$ meV. This is in good agreement with other measurements[22] and fits well to the theoretically expected trap depth of Cs and Pb vacancies inside the crystal lattice in the range of 200 meV.[19,21] Measurements on an additional sample are qualitatively consistent with these results, but yield larger trap depths hinting toward the presence of further point defects (see Figure S5, Supporting Information). It is also worth noting, that these traps could also be located at the grain boundary between individual NWs. Within the scope of these measurements, it is not possible to pinpoint neither the origin nor the location of these traps. Yet, measurements on single crystal samples show comparable or even higher values for N_{DT}, which is suggestive of an intrinsic origin of the traps.[12]

However, even in the presence of these substantial trap densities, the conductivity of the devices increase several orders of magnitude when illuminating the sample even at cryogenic temperatures (cf. Figure 3a,b). Notably, at low temperatures the conductivity even increases slowly with decreasing temperature. This peculiar behavior has also been seen in MALH system[56–58] and has led to an ongoing debate on its underlying mechanisms. Here, it is worth noting, that this change in the slope of the temperature dependence is not related to a phase transition temperature, even in MALH systems[56,57] In general, the photoconductivity depends on the absorption of the material, the mobility, and the charge carrier recombination rate.[56,57] However, some authors have argued, that charge carrier mobility variations are most probably the dominating parameter in this relation, although they were not able to measure the mobility directly.[56,57] The FET geometry employed within this study, however, allows for directly accessing the mobility in addition to the conductance. Figure 3c shows the mobility and Figure 3d shows a comparison of conductivity and mobility with respect to the (inverse) temperature. Additional data of further devices is shown in Figures S5 and S6, Supporting Information. As proposed by several authors,[56,57] the mobility indeed nicely mimics the photoconductivity behavior. In the low temperature regime, similar to the conductivity, the mobility increases with decreasing temperature. Such a behavior is a sign of charge carriers travelling in delocalized metal-like band states, where the mobility is limited by phonon scattering.[56,57] This transition from “semiconducting” to “metal-like” behavior is very surprising, especially given the existence of a high density of deep traps at that completely hindered transport in the dark. At higher temperatures, the mobility shows thermally activated behavior. By again using an Arrhenius relation for modeling the mobility $\mu \approx \exp(-E_A/k_BT)$, the activation energy can be calculated to be $E_A = 26 \pm 5$ meV (see Figure 3d). The activation energy of the illuminated sample is significantly lower than in the dark. Thus, at high temperatures, only shallow traps with a low activation energy influence charge transport. Besides, also excitons could be responsible for the thermally activated transport behavior. Their theoretically expected and measured binding energy of $E_B = 47$ meV[20,59,60] is in fair agreement with the thermal activation energy.

Figure 3e,f combines these results and shows an illustration of proposed transport mechanisms and energy landscape of the charge traps. Although the exact shape of the trap density of state remains unknown, the measurements indicate that it is composed of a high density of shallow traps together with a medium density of deep traps. In the dark (Figure 3e), a low density of charge carriers are induced by the gate. Since only a fraction of traps are filled, thermal activation of deep traps dominates transport. In illuminated samples (Figure 3f), however, a high density of photo-excited charge carriers are generated and deep traps are completely filled. In this case, at high temperatures only shallow traps influence charge transport. At low temperatures, also shallow traps freeze out enabling phonon-limited transport. This tolerance of charge transport in the bright state with respect to deep traps is remarkable. The suppressed influence of deep traps can also be seen as an extension to the notion of “defect tolerance” in perovskite materials that has only been connected to the presence of shallow traps so far.[19–23]

3. Conclusion

In summary, we have demonstrated the successful fabrication of $CsPbBr_3$ nanowire FET. Without illumination, we demonstrated a field effect with an on/off ratio of more than 10^4 and saturation mobilities reaching up to 4×10^{-3} cm^2 V^{-1} s^{-1} at room temperature. At the same time, photoconductivity with mobilities of up to 1.8×10^{-2} cm^2 V^{-1} s^{-1} and photoresponsivities of up to 25 A W^{-1} illustrate the promising phototransistor properties of $CsPbBr_3$ devices. Furthermore, transport properties down to cryogenic temperatures were investigated in detail. We showed that transport in the dark is dominated by deep traps and freezes out at low temperatures. Surprisingly, when switching on the illumination, excellent photoconductivity even exhibiting phonon-limited characteristics can be observed. This intriguing observation highlights and further extends the notion of the so-called “defect tolerance” of perovskite materials, since not only the influence of shallow traps but also of deep traps on the charge carrier mobility is completely suppressed in illuminated samples. Our findings provide further insight into defect states and enable a deeper understanding of charge transport in all-inorganic perovskite systems. They underline the superior optoelectronic properties of perovskite systems and indicate the importance of managing the density of deep traps in advancing the development of efficient optoelectronic devices especially for their use under low-light intensities.

4. Experimental Section

Synthesis of $CsPbB_3$ Nanowires: The synthesis was carried out following the previously reported ultrasonication approach.[15] In a typical synthesis, 1-octadecene (10 mL), oleylamine (0.5 mL), and oleic acid (0.5 mL) were sequentially added to a mixture of Cs_2CO_3 (0.1 mmol) and $PbBr_2$ (0.3 mmol) precursor powders and then subjected to tip-sonication

© 2021 The Authors. Advanced Electronic Materials published by Wiley-VCH GmbH

(Sonoplus HD 3100, Bandelin) at a power of 30 W for 60 min. The color of the reaction medium gradually turned into yellow during the course of the reaction. The resultant colloidal solution was centrifuged at a speed of 5000 rpm for 10 min. Then, the obtained sediment was dispersed in hexane (10 mL) under mild sonication. The centrifugation process was repeated thrice at a speed of 3000 rpm for 10 min. During this centrifugation process, the nanocubes present in the product separated from the NWs. At last, the sediment containing $CsPbBr_3$ NWs was dispersed in hexane (5 mL), which was used for the fabrication of devices. The optical properties of the as-prepared colloidal solutions were characterized by UV–VIS absorption (Cary60, Agilent Technologies) and photoluminescence (Varian Cary Eclipse, Agilent Technologies). The morphology of the obtained nanocrystals was characterized using a transmission electron microscope (JEM-1011, JEOL) operating at an accelerating voltage of 80–100 kV. The high-resolution high-angle annular dark field images were acquired using a scanning transmission electron microscope (Titan, FEI) operating at 300 kV.

Device Fabrication: For FET device fabrication, p-doped Si wafers with a 100 nm SiO_2 layer were used as substrates. First, the substrates were immersed in acetone and put into a sonicator for 3 min. Subsequently, the substrates were plasma-cleaned in O_2 plasma for 3 min (PICO Plasma Cleaner, Diener). The colloidal solution of $CsPbBr_3$ NWs was spin-coated onto the substrates at 1500 rpm for 1 min. Then, contact pads with a 0.3 nm titanium adhesion layer and a gold layer of 70 nm were evaporated on top of the perovskite film using a standard electron beam evaporation technique together with a shadow mask. The gold pads functioned as drain and source contacts, while the silicon substrate was used as a back-gate. Topography measurements were taken with an atomic force microscope (Dimension 3100, Bruker) in tapping mode. The thickness of the perovskite film was determined by measuring the step height of a scratch through the film.

Electrical Measurements: All electrical measurements were performed in a vacuum setup at $p < 5 \times 10^{-7}$ mbar (CRX-VF Probe Station, Lakeshore). Furthermore, the sample stage was thermally coupled to a helium pulse-tube refrigerator enabling measurements at a variable temperature in the range between 8 and 300 K. Two source/measure units (2450 SourceMeter, Keithley) were used to apply drain and gate voltages as well as to measure the respective currents. To investigate the photoresponse, a halogen lamp (Model 21AC, Techniquip) attached to the microscope of the probe station was employed. Wavelength-dependent measurements were conducted using two different laser diodes with a wavelength of 650 nm (532 nm) and a total power of 650 µW (548 µW).

Acknowledgements

R.T.W. acknowledges funding from the Center for Nanoscience (CeNS) and the Solar Technologies go Hybrid (SolTech) initiative as well as funding by the Deutsche Forschungsgemeinschaft (DFG, German Research Foundation) under Germany's Excellence Strategy-EXC-2111-390814868 (MCQST) and EXC 2089/1-390776260 (e-conversion). L.P. acknowledges financial support by the Bavarian State Ministry of Science, Research, and Arts through the grant "Solar Technologies go Hybrid (SolTech)."

Open Access funding enabled and organized by Projekt DEAL.

Conflict of Interest

The authors declare no conflict of interest.

Author Contributions

The manuscript was written through contributions of all authors. All authors have given approval to the final version of the manuscript.

Data Availability Statement

Research data are not shared.

Keywords

ceasium lead halide, charge transport, defects, field-effect transistors, perovskite nanowires, phototransistors

Received: January 31, 2021
Revised: March 3, 2021
Published online: May 6, 2021

[1] D. A. Valverde-Chávez, C. S. Ponseca, C. C. Stoumpos, A. Yartsev, M. G. Kanatzidis, V. Sundström, D. G. Cooke, *Energy Environ. Sci.* **2015**, *8*, 3700.
[2] J. S. Manser, P. V. Kamat, *Nat. Photonics* **2014**, *8*, 737.
[3] S. D. Stranks, G. E. Eperon, G. Grancini, C. Menelaou, M. J. P. Alcocer, T. Leijtens, L. M. Herz, A. Petrozza, H. J. Snaith, *Science* **2013**, *342*, 341.
[4] L. Polavarapu, B. Nickel, J. Feldmann, A. S. Urban, *Adv. Energy Mater.* **2017**, *7*, 1700267.
[5] M. M. Lee, J. Teuscher, T. Miyasaka, T. N. Murakami, H. J. Snaith, *Science* **2012**, *338*, 643.
[6] C. Xie, C.-K. Liu, H.-L. Loi, F. Yan, *Adv. Funct. Mater.* **2019**, *9*, 1903907.
[7] B. Yang, F. Zhang, J. Chen, S. Yang, X. Xia, T. Pullerits, W. Deng, K. Han, *Adv. Mater.* **2017**, *29*, 1703758.
[8] M. Shoaib, X. Zhang, X. Wang, H. Zhou, T. Xu, X. Wang, X. Hu, H. Liu, X. Fan, W. Zheng, T. Yang, S. Yang, Q. Zhang, X. Zhu, L. Sun, A. Pan, *J. Am. Chem. Soc.* **2017**, *139*, 15592.
[9] F. Li, C. Ma, H. Wang, W. Hu, W. Yu, A. D. Sheikh, T. Wu, *Nat. Commun.* **2015**, *6*, 8238.
[10] X. Y. Chin, D. Cortecchia, J. Yin, A. Bruno, C. Soci, *Nat. Commun.* **2015**, *6*, 7383.
[11] S. P. Senanayak, B. Yang, T. H. Thomas, N. Giesbrecht, W. Huang, E. Gann, B. Nair, K. Goedel, S. Guha, X. Moya, C. R. McNeill, P. Docampo, A. Sadhanala, R. H. Friend, H. Sirringhaus, *Sci. Adv.* **2017**, *3*, e1601935.
[12] Y. Zou, F. Li, C. Zhao, J. Xing, Z. Yu, W. Yu, C. Guo, *Adv. Opt. Mater.* **2019**, *7*, 1900676.
[13] H. Zhu, Y. Fu, F. Meng, X. Wu, Z. Gong, Q. Ding, M. V. Gustafsson, M. T. Trinh, S. Jin, X.-Y. Zhu, *Nat. Mater.* **2015**, *14*, 636.
[14] Y. Tong, M. Fu, E. Bladt, H. Huang, A. F. Richter, K. Wang, P. Müller-Buschbaum, S. Bals, P. Tamarat, B. Lounis, J. Feldmann, L. Polavarapu, *Angew. Chem., Int. Ed. Engl.* **2018**, *57*, 16094.
[15] Y. Tong, B. J. Bohn, E. Bladt, K. Wang, P. Müller-Buschbaum, S. Bals, A. S. Urban, L. Polavarapu, J. Feldmann, *Angew. Chem., Int. Ed. Engl.* **2017**, *56*, 13887.
[16] Y. Tong, E. Bladt, M. F. Aygüler, A. Manzi, K. Z. Milowska, V. A. Hintermayr, P. Docampo, S. Bals, A. S. Urban, L. Polavarapu, J. Feldmann, *Angew. Chem., Int. Ed. Engl.* **2016**, *55*, 13887.
[17] H. Huang, Y. Li, Y. Tong, E.-P. Yao, M. W. Feil, A. F. Richter, M. Döblinger, A. L. Rogach, J. Feldmann, L. Polavarapu, *Angew. Chem., Int. Ed. Engl.* **2019**, *58*, 16558.
[18] X. Zhang, S. Chen, X. Wang, A. Pan, *Small Methods* **2019**, *3*, 1800294.
[19] J. Kang, L.-W. Wang, *J. Phys. Chem. Lett.* **2017**, *8*, 489.
[20] Y. Jiang, X. Wang, A. Pan, *Adv. Mater.* **2019**, *31*, e1806671.
[21] H. Jin, E. Debroye, M. Keshavarz, I. G. Scheblykin, M. B. J. Roeffaers, J. Hofkens, J. A. Steele, *Mater. Horiz.* **2020**, *7*, 397.

© 2021 The Authors. Advanced Electronic Materials published by Wiley-VCH GmbH

[22] M. Bruzzi, F. Gabelloni, N. Calisi, S. Caporali, A. Vinattieri, *Nanomaterials* **2019**, *9*, 177.
[23] A. Zakutayev, C. M. Caskey, A. N. Fioretti, D. S. Ginley, J. Vidal, V. Stevanovic, E. Tea, S. Lany, *J. Phys. Chem. Lett.* **2014**, *5*, 1117.
[24] C. R. Kagan, D. B. Mitzi, C. D. Dimitrakopoulos, *Science* **1999**, *286*, 945.
[25] D. Li, G. Wang, H.-C. Cheng, C.-Y. Chen, H. Wu, Y. Liu, Y. Huang, X. Duan, *Nat. Commun.* **2016**, *7*, 11330.
[26] W. Yu, F. Li, L. Yu, M. R. Niazi, Y. Zou, D. Corzo, A. Basu, C. Ma, S. Dey, M. L. Tietze, U. Buttner, X. Wang, Z. Wang, M. N. Hedhili, C. Guo, T. Wu, A. Amassian, *Nat. Commun.* **2018**, *9*, 5354.
[27] E. Oksenberg, E. Sanders, R. Popovitz-Biro, L. Houben, E. Joselevich, *Nano Lett.* **2018**, *18*, 424.
[28] C. Huo, X. Liu, X. Song, Z. Wang, H. Zeng, *J. Phys. Chem. Lett.* **2017**, *8*, 4785.
[29] X. Hu, H. Zhou, Z. Jiang, X. Wang, S. Yuan, J. Lan, Y. Fu, X. Zhang, W. Zheng, X. Wang, X. Zhu, L. Liao, G. Xu, S. Jin, A. Pan, *ACS Nano* **2017**, *11*, 9869.
[30] J. Kim, S.-H. Lee, J. H. Lee, K.-H. Hong, *J. Phys. Chem. Lett.* **2014**, *5*, 1312.
[31] Q. Wang, Y. Shao, H. Xie, L. Lyu, X. Liu, Y. Gao, J. Huang, *Appl. Phys. Lett.* **2014**, *105*, 163508.
[32] W. L. Leong, Z.-E. Ooi, D. Sabba, C. Yi, S. M. Zakeeruddin, M. Graetzel, J. M. Gordon, E. A. Katz, N. Mathews, *Adv. Mater.* **2016**, *28*, 2439.
[33] T. Zhang, C. Hu, S. Yang, *Small Methods* **2019**, *4*, 1900552.
[34] R. T. Weitz, U. Zschieschang, F. Effenberger, H. Klauk, M. Burghard, K. Kern, *Nano Lett.* **2007**, *7*, 22.
[35] Z. Xiao, Y. Yuan, Y. Shao, Q. Wang, Q. Dong, C. Bi, P. Sharma, A. Gruverman, J. Huang, *Nat. Mater.* **2015**, *14*, 193.
[36] B.-B. Zhang, F. Wang, H. Zhang, B. Xiao, Q. Sun, J. Guo, A. B. Hafsia, A. Shao, Y. Xu, J. Zhou, *Appl. Phys. Lett.* **2020**, *116*, 63505.
[37] C. Chen, Q. Fu, P. Guo, H. Chen, M. Wang, W. Luo, Z. Zheng, *Mater. Res. Express* **2019**, *6*, 115808.
[38] C. Eames, J. M. Frost, P. R. F. Barnes, B. C. O'Regan, A. Walsh, M. S. Islam, *Nat. Commun.* **2015**, *6*, 7497.
[39] Y. Meng, C. Lan, F. Li, S. Yip, R. Wei, X. Kang, X. Bu, R. Dong, H. Zhang, J. C. Ho, *ACS Nano* **2019**, *13*, 6060.
[40] X. Hu, X. Wang, P. Fan, Y. Li, X. Zhang, Q. Liu, W. Zheng, G. Xu, X. Wang, X. Zhu, A. Pan, *Nano Lett.* **2018**, *18*, 3024.
[41] L. Janker, Y. Tong, L. Polavarapu, J. Feldmann, A. S. Urban, H. J. Krenner, *Nano Lett.* **2019**, *19*, 8701.
[42] H. Zhang, X. Liu, J. Dong, H. Yu, C. Zhou, B. Zhang, Y. Xu, W. Jie, *Cryst. Growth Des.* **2017**, *17*, 6426.
[43] G. R. Yettapu, D. Talukdar, S. Sarkar, A. Swarnkar, A. Nag, P. Ghosh, P. Mandal, *Nano Lett.* **2016**, *16*, 4838.
[44] A. Jha, H.-G. Duan, V. Tiwari, P. K. Nayak, H. J. Snaith, M. Thorwart, R. J. D. Miller, *ACS Photonics* **2017**, *5*, 852.
[45] Y. Chen, H. T. Yi, X. Wu, R. Haroldson, Y. N. Gartstein, Y. I. Rodionov, K. S. Tikhonov, A. Zakhidov, X.-Y. Zhu, V. Podzorov, *Nat. Commun.* **2016**, *7*, 12253.
[46] M. Buscema, J. O. Island, D. J. Groenendijk, S. I. Blanter, G. A. Steele, H. S. J. van der Zant, A. Castellanos-Gomez, *Chem. Soc. Rev.* **2015**, *44*, 3691.
[47] J. Feng, X. Yan, Y. Liu, H. Gao, Y. Wu, B. Su, L. Jiang, *Adv. Mater.* **2017**, *29*, 1605993.
[48] P. Stallinga, *Electrical Characterization of Organic Electronic Materials and Devices*, John Wiley & Sons Ltd., Chichester, UK **2009**.
[49] H. F. Haneef, A. M. Zeidell, O. D. Jurchescu, *J. Mater. Chem. C* **2020**, *8*, 759.
[50] M. Waldrip, O. D. Jurchescu, D. J. Gundlach, E. G. Bittle, *Adv. Funct. Mater.* **2019**, *39*, 1904576.
[51] Y. Xu, H. Sun, W. Li, Y.-F. Lin, F. Balestra, G. Ghibaudo, Y.-Y. Noh, *Adv. Mater.* **2017**, *29*, 1702729.
[52] L. Bürgi, T. J. Richards, R. H. Friend, H. Sirringhaus, *J. Appl. Phys.* **2003**, *94*, 6129.
[53] C. C. Stoumpos, C. D. Malliakas, J. A. Peters, Z. Liu, M. Sebastian, J. Im, T. C. Chasapis, A. C. Wibowo, D. Y. Chung, A. J. Freeman, B. W. Wessels, M. G. Kanatzidis, *Cryst. Growth Des.* **2013**, *13*, 2722.
[54] S. Hirotsu, J. Harada, M. Iizumi, K. Gesi, *J. Phys. Soc. Jpn.* **1974**, *37*, 1393.
[55] V. Podzorov, E. Menard, A. Borissov, V. Kiryukhin, J. A. Rogers, M. E. Gershenson, *Phys. Rev. Lett.* **2004**, *93*, 86602.
[56] M. V. Khenkin, D. V. Amasev, S. A. Kozyukhin, A. V. Sadovnikov, E. A. Katz, A. G. Kazanskii, *Appl. Phys. Lett.* **2017**, *110*, 222107.
[57] A. Pisoni, J. Jacimovic, B. Náfrádi, P. Szirmai, M. Spina, R. Gaál, K. Holczer, E. Tutis, L. Forró, E. Horváth, arXiv:1604.05637 **2016**.
[58] D. V. Amasev, A. R. Tameev, A. G. Kazanskii, *Semiconductors* **2019**, *53*, 1597.
[59] B. T. Diroll, H. Zhou, R. D. Schaller, *Adv. Funct. Mater.* **2018**, *28*, 1800945.
[60] Q. Zhang, R. Su, X. Liu, J. Xing, T. C. Sum, Q. Xiong, *Adv. Funct. Mater.* **2016**, *26*, 6238.

© 2021 The Authors. Advanced Electronic Materials published by Wiley-VCH GmbH